Differential and total cross sections for charge transfer and transfer-excitation in ion-helium collisions

S. Halder,[1] A. Mondal,[2] S. Samaddar,[1] C. R. Mandal,[1] and M. Purkait[1,*]

[1]*Department of Physics, Ramakrishna Mission Residential College, Narendrapur, Kolkata 700103, India*

[2]*Department of Physics, Ramsaday College, Amta, Howrah 711401, India*

(Received 24 May 2017; revised manuscript received 7 August 2017; published 26 September 2017)

Total cross sections for single charge transfer in collisions of multicharged bare ions with ground-state helium atoms at incident energy ranging from 40 to 5000 keV/amu have been calculated in the framework of a four-body model of final channel distorted-wave (FC-DW-4B) approximation. In this formalism, distortion in the final channel related to the Coulomb continuum of the target and the Coulomb interaction between the passive electron in the target with the projectile are included. In all cases, total single electron-capture cross sections have been calculated by summing over all contributions up to $n = 3$ shells and subshells. It has been observed that the contribution of the capture cross sections into excited states have insignificant contributions for symmetric collisions. Comprehensive comparisons are made between the four body model of boundary corrected continuum intermediate-state approximations [Phys. Rev. A **83**, 032706 (2011)] and the present FC-DW-4B model. The main purpose of the present study is to investigate the relative importance of dynamic electron correlation and the role of passive electron in the target at intermediate and high impact energies. In addition, projectile angular differential cross sections (DCS) for charge transfer and transfer-excitation in p-He collisions are calculated at different impact energies. At low projectile energies, the present DCS data exhibits the typical steeply decreasing dependence on the projectile scattering angles, whereas at high impact energies, the double-scattering region centered on the Thomas angle is obtained. Detailed comparisons with the available experimental data and other theories are reported with the purpose of further assessing the relevance of the present model at different impact energies. Overall, the calculated cross sections show good agreement with the available experimental findings.

DOI: 10.1103/PhysRevA.96.032717

I. INTRODUCTION

Electron capture from multielectron target atoms by the impact of multicharged bare ions has received considerable attention over a long period of time from both experimental and theoretical points of view for their practical applications in plasma physics, astrophysics, controlled thermonuclear fusion research, and medical accelerators, etc. The dynamics of entangled many-body Coulomb systems is still one of the most fundamental challenges in atomic collision physics. Even in the simplest test case, the dynamics of the three-body Coulomb problem has yet to be fully understood. Since helium is the simplest multielectronic atom existing in nature, it offers a unique opportunity to understand the complex dynamics of many-particle collisions from both the experimental and theoretical investigations. The theoretical descriptions of single-electron capture from multielectronic targets in interaction with fast bare ions become complicated due to the presence of many electrons. Usually, it is performed by reducing the many-body problem to one of the three interacting particles; the projectile, the active electron, and the residual target. In this three-body approximation, a given active electron moves under the combined field of the projectile and the residual target considering that the other target electrons remain frozen in their initial states. This approximation is known as frozen-core approximation. Such an approximation is a reduction of a many-body problem to a three-body problem. In the case where two electrons actively take part in the collision, the challenge for theory is significantly increased since a four-body approach is required. The three-body process of single charge transfer [or single capture (SC)] has been studied intensively [1-12], and several reviews of this work have been published [13-17]. For a long time, theoretical and experimental efforts concentrated on the energy dependence of total cross sections (TCS) as well as differential cross sections (DCS). Different theories such as the four-body formalism of the continuum distorted wave (CDW-4B) [18-19], the Born distorted wave (BDW-4B) [20,21], the continuum distorted wave-eikonal initial state (CDW-EIS) [22], the CDW Born final state (CDW-BFS) and the CDW Born initial state (CDW-BIS) [23-24], the two-center basic generator method (TC-BGM) [25-26], the boundary corrected first Born (CB1-4B) [27-30], the boundary corrected continuum intermediate state (BCCIS-4B) [31-34], and the Coulomb Born distorted wave (CBDW-4B) [35-38] approximations have been developed to study the electron transfer and transfer-excitation (TE) by multicharged bare ion with ground-state helium. In this theoretical study, we have concentrated our efforts on the determination of cross sections for electron transfer and transfer-excitation of helium atom in the ground state by the impact of multicharged bare ions using the four-body model of final channel distorted-wave (FC-DW-4B) approximation at intermediate and high energies.

The single electron-capture process for p-He collisions is the dominant channel and the Thomas double-scattering mechanism is well known to have a negligible contribution to this process at intermediate and low collision energy [39], where the projectile velocity is comparable to or smaller than the velocity of electron in the target. In the intermediate- and high-energy region, the pure single electron-capture (SC) and transfer-excitation (TE) processes are of particular interest.

*Corresponding author: mpurkait_2007@rediffmail.com, rkmcnpur@vsnl.com

The former is a pure one-electron system where one active electron in the target is captured to the projectile and the other electron remains in the ground state of the target. The later involves the capture of one target electron into the projectile with simultaneous excitation of the other electron in the target. However, in the TE process both the electrons are actively involved. In most of the theoretical investigations, the transfer into excited state or the transfer combined with a target excitation of a second electron were neglected. Using a reaction microscope, Hasan *et al.* [40] first studied the transfer-excitation (TE) in intermediate energy range (25–75 keV) for p-He collisions. In this work, they have shown the comparisons between TE and double excitation cross sections which indicate the dynamic couplings between the nucleus-electron and/or electron-electron correlation in ion-atom collision. The followup investigation by Schulz *et al.* [41] reported differential double and single electron-capture cross sections in the energy range from 15 to 150 keV for p-He collisions. Following these experimental results, Zapukhlyak *et al.* [25] calculated in details of the projectile angular differential cross sections for SC and TE in the energy range from 5 to 200 keV for proton-helium collisions in the framework of two-center extension of the nonperturbative basis generator method (TC-BGM). We see that, for SC, the TC-BGM calculations show overall good agreement with the above-mentioned experimental results. In the case of TE, the agreement between the TC-BGM calculation and the measurement are not in satisfactory agreement. Such discrepancies may originate from the quantum mechanical heavy-particle-electron couplings instead of the electron-electron-correlation effects. Schoffler *et al.* [42-43] have measured the state selective angular-differential cross sections for SC and double capture (DC) in collisions of p and $He^{1,2+}$ projectiles with a helium for incident energies of 60–630 keV/amu. They have also reported theoretical results obtained by means of CDW-BFF and CDW-BIS approximations [23-24]. Later, Zapukhlyak and Kirchner [26] calculated the projectile angular-differential cross sections for the processes using TC-BGM with the independent electron model (IEM) and compared the results with the experimental data [42-43]. They have concluded that electron correlations play a negligible role in the processes. Recently, Guo *et al.* [44] have measured state-selective electron-capture cross sections and projectile scattering–angular differential cross sections for SC and TE in collisions of proton with He at energies ranging from 50 to 100 keV by means of a reaction microscope. They have shown that the ground-state capture is the dominant reaction channel, and excited-state transfer has relatively small contributions to the cross sections for SC. The TE process has a minor contribution to the total cross sections. In addition, the electron-electron-correlation effects, which are negligible in the SC process, manifest their importance in the TE process. Recently, Belkic and his group [28-30] have extensively investigated the TCS and DCS for SC in collisions of p-He collisions at intermediate and high energies. The calculations have been carried out by means of the four-body boundary corrected continuum intermediate state (BCIS-4B)and the first Born (CB1-4B) approximation. In such study, they have found the clear double-scattering process (Thomas process) with increasing projectile energy in the DCS results. In addition, they have also investigated the role of two electrons in the target and intermediate ionization continua in the problem of single electron capture from helium atom at intermediate and high energies. In the present study, the four-body model of final channel distorted-wave (FC-DW-4B) approximation has been employed to study the above-mentioned processes (both SC and TE) in collisions of multicharged bare ions with a helium atom at intermediate and high energies.

The organization of this paper is as follows. Section II contains the theoretical calculations of the problem. Our results and discussions are presented in Sec. III. Finally, concluding remarks are given in Sec. IV. Atomic units have been used throughout the work.

II. THEORY

In this section, theoretical formulation for projectile-angular differential cross sections as well as total cross sections for SC and TE process is presented using the (FC-DW-4B) approximation. Single electron-capture (SC) and transfer-excitation (TE) process in collisions of bare ions with helium atom may be represented as

$$X_P^{q+}(q{=}1,2,3,5,6,8) + \mathrm{He}_T(1s^2) \rightarrow X_P^{(q-1)+}(nl) + \mathrm{He}_T^{+}(1s) \tag{1}$$

and

$$X_P^{q+}(q=1) + \mathrm{He}_T(1s^2) \rightarrow X_P^{(q-1)+}(1s) + \mathrm{He}_T^{+}(nl). \tag{2}$$

Here we consider a collision between a bare projectile (X_P^{q+}) of charge Z_P^q and heliumlike target system (T) consisting of two electrons e_1 and e_2 initially bound to the target nucleus of charge Z_T. $\vec{s}_{1,2}$ and $\vec{x}_{1,2}$ have been leveled as the position vectors of the electrons $e_{1,2}$ relative to Z_P and Z_T, respectively. The interelectron coordinate is denoted by $\vec{r}_{12} = \vec{s}_1 - \vec{s}_2 = \vec{x}_1 - \vec{x}_2$. $\vec{R}$ denotes the position vector of the projectile (P) relative to the target (T) nucleus. In the entrance channel, it is convenient to introduce $\vec{r}_i$ as the position vector of the projectile (P) with respect to the center of mass of the helium target. In the exit channel, $\vec{r}_f$ is the position vector of the center of mass of (X_P^{q+},e_1) with respect to the center of mass of (He^+,e_2). The position vectors $\vec{r}_i$ and $\vec{r}_f$ are given by

$$\vec{r}_i = \vec{R} - \frac{m_e}{2m_e + M_T}(\vec{x}_1 + \vec{x}_2) \tag{3}$$

and

$$\vec{r}_f = \frac{m_e M_P}{m_e + M_P}\vec{R} + \frac{m_e}{m_e + M_P}\vec{x}_1 - \frac{m_e}{m_e + M_T}\vec{x}_2, \tag{4}$$

where m_e, M_T, and M_P are the masses of the electron, target, and projectile, respectively. The scattering amplitude in the distorted-wave formalism may be written as

$$T_{if} = \langle \psi_f^- | V_i | \psi_i \rangle, \tag{5}$$

where $\psi_f^-(\psi_i)$ is an approximate final- (initial-) state wave function, and V_i is the initial-state projectile-atom interaction. The initial projectile-atom interaction is given by

$$V_i = \frac{Z_P Z_T}{R} - \frac{Z_P}{s_1} - \frac{Z_P}{s_2}. \tag{6}$$

We approximate the initial-state wave function as

$$\psi_i = \chi_i(\vec{r}_i)\phi_{He}(\vec{x}_1,\vec{x}_2), \tag{7}$$

where $\chi_i(\vec{r})$ is the unperturbed wave function for the incident projectile and $\phi_{He}(\vec{x}_1,\vec{x}_2)$ is a four-parameter wave function of Lowdin [45], given by

$$\phi_{He}(\vec{x}_1,\vec{x}_2) = N(a_1 e^{-\alpha_1 x_1} + a_2 e^{-\alpha_2 x_1})(a_1 e^{-\alpha_1 x_2} + a_2 e^{-\alpha_2 x_2}), \tag{8}$$

where $a_1 = 2.7626$, $a_2 = 1.9104$, $\alpha_1 = 1.4287$, $\alpha_2 = 2.7022$, and $\epsilon_i = -2.861525$. The incident projectile plane wave is given by

$$\chi_i(\vec{r}_i) = e^{i\vec{k}_i\cdot\vec{r}_i}, \tag{9}$$

where k_i is the relative momentum of the projectile with respect to center of mass of the target in the initial channel. The final-state wave function is approximated as

$$\psi_f^- = \chi_f^-(\vec{r}_f)\phi_P(\vec{s}_1)\phi_{He^+}(\vec{x}_2)C_{T-e_1}(\vec{x}_1)C_{P-e_2}(\vec{s}_2), \tag{10}$$

where $C_{P-e_2}(\vec{s}_2)$ represents the Coulomb interaction between the projectile and the noncaptured electron in the target and $C_{T-e_1}(\vec{x}_1)$ represents the interaction between the target nucleus and the captured electron. The final-state wave function of $\phi_P(\vec{s}_1)$ and $\phi_{He^+}(\vec{x}_2)$ are hydrogenic which are known exactly. The scattered wave function of the projectile is approximated by a Coulomb wave which may be given by

$$\chi_f^-(\vec{r}_f) = e^{i\vec{k}_f\cdot\vec{r}_f} e^{-\frac{\pi}{2}\gamma_3}\Gamma(1-i\gamma_3)\,{}_1F_1\{i\gamma_3,1;-i(\vec{k}_f\cdot\vec{r}_f + k_f r_f)\}, \tag{11}$$

where $\vec{k}_f$ is the relative momentum of the projectile with respect to the center of mass of target in the final channel. Here γ_3 is the Sommerfeld parameter which is given by $\gamma_3 = \frac{Z_P Z_T}{v_f}$, with v_f being the velocity of the outgoing projectile. The two particle interactions are the Coulomb distortion factor which is given by

$$C_{T-e_1}(\vec{x}_1) = e^{\frac{\pi}{2}\gamma_1}\Gamma(1+i\gamma_1)\,{}_1F_1\{-i\gamma_1,1;-i(\vec{v}_f\cdot\vec{x}_1 + v_f x_1)\} \tag{12}$$

and

$$C_{P-e_2}(\vec{s}_2) = e^{\frac{\pi}{2}\gamma_2}\Gamma(1+i\gamma_2)\,{}_1F_1\{-i\vec{s}_2,1;-i(\vec{v}_f\cdot\vec{s}_2 + v_f s_2)\}, \tag{13}$$

with $\gamma_1 = \frac{Z_T}{v_f}$ and $\gamma_2 = \frac{Z_P}{v_f}$. The transition amplitudes for SC and TE in the FCDW-4B theory may be written as

$$T_{if} = N\iiint d\vec{x}_1 d\vec{x}_2 d\vec{R}\, e^{i\vec{k}_i\cdot\vec{r}_i - i\vec{k}_f\cdot\vec{r}_f}\,{}_1F_1\{i\gamma_1;1;i(\vec{v}_f\cdot\vec{x}_1 + v_f x_1)\}\,{}_1F_1\{i\gamma_2;1;i(\vec{v}_f\cdot\vec{s}_2 + v_f s_2)\}$$
$$\times\,{}_1F_1\{-i\gamma_3;1;i(\vec{k}_f\cdot\vec{r}_f + k_f r_f)\}\left(\frac{Z_P Z_T}{R} - \frac{Z_P}{s_1} - \frac{Z_P}{s_2}\right)\phi_{He}(\vec{x}_1,\vec{x}_2)\phi^*_{He^+}(\vec{x}_2)\phi^*_P(\vec{s}_1), \tag{14}$$

where $N = e^{\frac{\pi}{2}(\gamma_1+\gamma_2-\gamma_3)}\Gamma(1-i\gamma_1)\Gamma(1+i\gamma_3)\Gamma(1-i\gamma_2)$. For the confluent hypergeometric function, we use the contour integral representation [46]

$${}_1F_1(i\gamma,1,z) = \frac{1}{2\pi i}\oint_\Gamma^{0+,1+} s(\gamma,u)e^{zu}du, \tag{15}$$

where $s(\gamma,u) = u^{-1+i\gamma}(u-1)^{-i\gamma}$,$s(\gamma,t)$ is single valued and analytic over the contour Γ enclosing zero and 1 once counterclockwise resulting in a branch cut from zero to 1. The phase convention is as follows: the phase of a complex variable z is to be taken as zero on the positive real axis from which it is counted as positive when counterclockwise and negative when clockwise, thereby forming a cut from zero to $-\infty$ on the real axis. Using this representation, we may express the equation (14) as

$$T_{if} = \frac{N}{(2\pi i)^2}\oint_{\Gamma_2}^{0+,1+}\oint_{\Gamma_3}^{0+,1+} du_2 du_3 s(\gamma_2,u_2)s(\gamma_3,u_3)\,{}_1F_1(i\gamma_1,1,i(\vec{v}_f\cdot\vec{x}_1 + v_f\cdot x_1)J', \tag{16}$$

where

$$J' = \iiint d\vec{x}_1 d\vec{x}_2 d\vec{R}\, e^{i\vec{k}_i\cdot\vec{r}_i - \vec{k}_f\cdot\vec{r}_f + iu_2(\vec{v}_f\cdot\vec{s}_2 + v_f s_2) + iu_3(\vec{k}_f\cdot\vec{r}_f + k_f r_f)}\phi_{He}(\vec{x}_1\cdot\vec{x}_2)\times\phi^*_{He^+}(\vec{x}_2)\phi^*_P(\vec{s}_1)\left(\frac{Z_P Z_T}{R} - \frac{Z_P}{s_1} - \frac{Z_P}{s_2}\right). \tag{17}$$

We utilize the integral representation of the hypergeometric function

$${}_1F_1\{i\gamma_1;1;i(\vec{v}_f\cdot\vec{x}_1 + v_f x_1)\} = \frac{1}{\Gamma i\gamma_1\Gamma(1-i\gamma_1)}\int_0^1 du_1 u_1^{(i\gamma_1-1)}(1-u_1)^{-i\gamma_1}e^{i(\vec{v}_f\vec{x}_1 + v_f x_1)u_1}. \tag{18}$$

Thus the equation (16) can be written in the following form:

$$T_{if} = \frac{1}{(2\pi i)^2}\frac{N}{\Gamma(i\gamma_1)\Gamma(1-i\gamma_1)}\int_0^1 du_1 u_1^{i\gamma_1-1}(1-u_1)^{-i\gamma_1}\oint_{\Gamma_2}^{0+,1+}\oint_{\Gamma_3}^{0+,1+} du_2 du_3 s(\gamma_2,u_2)s(\gamma_3,u_3)J'', \tag{19}$$

where

$$J'' = Z_P\left(\frac{Z_T\partial^4}{\partial\delta_1\partial\delta_2\partial\lambda_1\partial\lambda_i} - \frac{\partial^4}{\partial\delta_1\partial\delta_2\partial\lambda_1\partial\epsilon_i} - \frac{\partial^4}{\partial\delta_1\partial\delta_2\partial\lambda_1\partial\lambda_i}\right)J_0. \tag{20}$$

Here

$$J_0 = A\lim_{\lambda_i,\epsilon_i\to 0}\iiint d\vec{x}_1 d\vec{x}_2 d\vec{R}\frac{e^{-\beta_1 x_1}}{x_1}\frac{e^{-\beta_2 x_1}}{x_2}\frac{e^{-\lambda_1 s_1}}{s_1}\frac{e^{-\lambda_2 s_2}}{s_2}e^{\vec{M}_1\cdot\vec{R}+\vec{M}_2\cdot\vec{x}_1+\vec{M}_3\cdot\vec{x}_2+\vec{M}_4\cdot\vec{s}_2} \tag{21}$$

and $\vec{M}_1 = \vec{k}_i - b\vec{k}_f + \vec{k}_f u_3$, $\vec{M}_2 = -a_2\vec{k}_i - b_1\vec{k}_f + \vec{v}_f u_1$, $\vec{M}_4 = \vec{v}_f u_2$, $\vec{M}_3 = -a_2\vec{k}_i - a_1\vec{k}_f$, with $a_1 = \frac{m_e}{m_e+M_T}$, $b_1 = \frac{m_e}{m_e+M_P}$, $b = \frac{M_P m_e}{m_e+M_P}$, $a_2 = \frac{m_e}{2m_e+M_T}$, $\beta_1 = \delta_1 - iv_f u_1$, $\beta_2 = \delta_2 + \delta_2'$, $\lambda_2 = \lambda_i - iv_f u_2$, and $\epsilon = \epsilon_i - ik_f u_3$.

We introduced the parameters ϵ_i and λ_i for the convenience of our calculation. Here δ_1, δ_2, δ_2', and λ_1 are the orbital component of the initial and final bound-state wave functions. The constant A originates from the initial and final bound-state wave functions. Using the Feynman parametrization integral, we may use the following identity as

$$\frac{1}{a^s b^r} = \frac{(s+r-1)!}{(s-1)!(r-1)!}\int_0^1 dt\frac{t^{s-1}(1-t)^{r-1}}{[at+b(1-t)]^{s+r}}, \tag{22}$$

Using Fourier transform technique and following three denominator Lewis integral [47], the space integration of J_0 of Eq. (21) can be reduced following Sinha and Sil [48] as

$$J_0 = 32\pi^2\int_0^1\int_0^\infty \frac{dv}{X_0 + X_1u_2 + X_2u_3 + X_3u_2u_3}, \tag{23}$$

where Δ, X_0, X_1, X_2, and X_3 are functions of the momentum masses, velocities, orbital components of the bound state, and the integration variables t, u_1, and v, respectively. The Feyman integral from zero to 1 and the Lewis integral with infinite upper limit have been calculated numerically by the 36-point and 46-point Gauss-Legendre quadrature method, respectively. Analogous to our previous work [32,33,49] we get the final transition amplitude which contained three-dimensional integrals such as Lewis, Feyman, and other integral of variable u_1. The other integration variable is u_1 from zero to 1 which has been integrated numerically by the 36-point Gauss Legendre quadrature method [30]. The details are found elsewhere [32,33,49]. The differential cross sections (DCS) for SC and TC process are given by

$$\frac{d\sigma}{d\Omega_P} = \frac{\mu_i\mu_f}{(2\pi)^2}\frac{k_i}{k_f}|T_{if}|^2, \tag{24}$$

where $\mu_i = \frac{M_P(2m_e+M_T)}{2m_e+M_P+M_T}$, $\mu_f = \frac{(m_e+M_P)(m_e+M_T)}{2m_e+M_P+M_T}$, and T_{if} is the transition amplitude under consideration.

Consequently, the total cross section (TCS) is

$$\sigma_{\text{total}} = \frac{\mu_i\mu_f}{(2\pi)^2}\frac{k_i}{k_f}\int|T_{if}|^2 d\Omega_P. \tag{25}$$

Here Ω_P is the solid angle of the projectile with respect to the direction of the incident projectile. Finally, the TCS for SC is obtained by numerical integration over the projectile scattering angle.

III. RESULTS AND DISCUSSION

We have calculated the cross sections for SC and TE in collisions of multicharged bare projectile ions with He at intermediate and high impact energies. A four-body final channel distorted-wave theory termed as the FC-DW-4B method is employed to calculate the differential cross sections (DCS) for only p-He collision and total cross sections (TCS) for fully striped bare projectile ions of different charge state (q = 1–3,5,6,8) with He. The TCS are obtained by summing over all contributions from individual shells and subshells up to $n = 3$. The variation of TCS for SC by the impact of different projectile ions as a function of the incident energy 40 to 5000 keV/amu is plotted in Figs. 1–6, respectively, using the postform of BCCIS-4B [32] and the present FC-DW-4B approximation. In addition, theoretical results for DCS of SC and TE processes in p-He collision are shown in Figs. 7–14, respectively, at intermediate and high energies.

A. Total cross sections

The total cross sections (TCS) results obtained from FC-DW-4B for p-He collision at incident energy ranging from 30 to 1000 keV are presented in Fig. 1. Our computed results

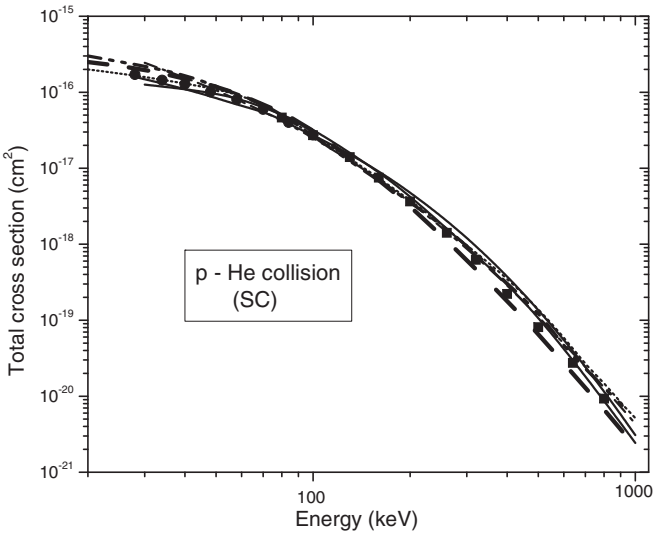

FIG. 1. Variation of total cross sections (TCS) for SC as a function of incident projectile energy for p-He collision. The solid curve presents FC-DW-4B results; dashed curve, BCCIS-4B results [34]; dotted curve, TCDW-4B results [43]; dash-dotted curve, CB1-4B results [27]; dash-dot-dotted curve, CDW-BIS results [24]; short-dotted curve, TCBGM results [25]. Experimental data: solid circle, results of Shah *et al.* [50]; solid square, Shah and Gilbody [51].

have been compared with the theoretical results of CDW-BIS [24], TC-BGM [25], CB1-4B [27], BCCIS-4B [34], the four-body model of target continuum distorted-wave (TCDW-4B) [49] approximation, and with the measurements [50,51]. The agreement between FC-DW-4B theory and experimental results are found to be satisfactory in low and intermediate energy ranges. This may be due to the inclusion of distortion in the final channel related to the Coulomb continuum states of the active electron in the field of residual target ion along with the Coulomb interaction between the projectile and the passive electron in the helium ion. The results obtained in the postform of BCCIS-4B (dashed curve) have good agreement with the experimental findings between 80 and 1000 keV. The BCCIS-4B method also includes full account of the Coulomb continuum states of the projectile ion and the active electron in the field of residual target ion in the final channel. The theoretical results of Mancev and Milojevic [27] using the CB1-4B approximation (dotted curve) and the CDW-BIS results of Mancev [24] (dash-dot-dotted curve) overestimate the observed cross sections in low-energy range (below 80 keV). This is expected because the formulation may not work well in this energy region. However, the CDW-BIS method takes full account of the Coulomb intermediate state of the captured electron only in one channel, i.e., in the exit channel. Here we may also note that the computed results have excellent agreement with the theoretical results of Zapukhlyak *et al.* [25] (short dotted curve) and the TCDW-4B results (dotted curve) of Samaddar *et al.* [49] along with experiments [50,51] in the whole energy range considered. In the TCDW-4B model, only the inclusion of continuum interaction of the active electron with the target in the exit channel are taken. In Fig. 2, we present our theoretical

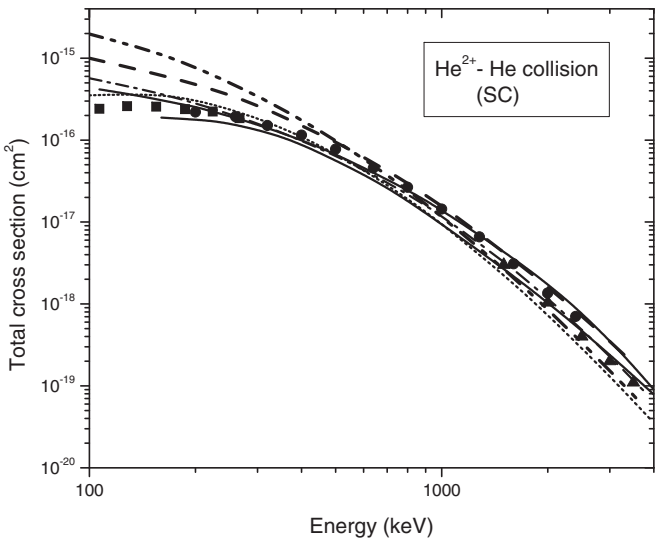

FIG. 2. Variation of total cross sections (TCS) for SC as a function of incident projectile energy for He^{2+}-He collision. The solid curve presents FC-DW-4B results; dashed curve, BCCIS-4B results [32]; dotted curve, TCDW-4B results [49]; dash-dotted curve, CB1-4B results [27]; dash-dot-dotted curve, CDW-4B results [53]; short-dotted curve, BDW-4B results [20]. Experimental data: solid square, results of Shah *et al.* [50]; solid circle, Shah and Gilbody [51]; solid triangle, de Castro *et al.* [52].

values for the TCS in the energy region 100 keV to 4 MeV for He^{2+}-He collision and have compared them with the experimental results [50,51,52] and other theoretical results [20,27,32,39,53]. The present results obtained by FC-DW-4B approximation are found to be in excellent agreement with experimental results throughout the energy region specially in the lower energy range, whereas the BCCIS-4B cross sections [32] (dashed curve) grossly overestimate the TCS in the lower energy region below 250 keV/amu and are in good harmony with the experimental results of de Castro *et al.* [52] at high energies. We find that the four-body Born distorted-wave (BDW-4B) results of Mancev [20] (short-dotted curve) give quite good agreement in the low- and intermediate-energy region. On the other hand, the CDW-4B results of Mancev [53] (dash-dot-dotted curve) yields unphysically large cross sections at lower energies. The BDW-4B and CDW-4B cross sections are very close to each other at higher impact energies. However, the CDW-4B approximation incorporates two Coulomb waves for the capture electron in both entrance and exit channels, whereas the BDW-4B method is four-body one-channel distorted-wave theory. Hence an overemphasis of two continuum states in both channels invalidates the CDW-4B method for SC in comparison with experimental data at lower impact energies. Thus we should expect that the electronic intermediate ionization states in one channel yield good results at lower energies. The same behavior is also obtained in the present theoretical model where the electronic ionization continua in the final channel is taken. It may also be observed from Fig. 2 that the CB1-4B results (dash-dotted curve) overestimate the experimental results of Shah *et al.* [50] at energies below 200 keV. However, the theoretical results move towards the experimental data as the impact energy increases. This may indicate that the dynamic electron correlation plays a very important role, expecially at higher impact energies. A similar conclusion has been previously reached in Refs. [11,19] by using CDW-4B and BCCIS-4B models for the same collision system. The TCS results for single transfer process in Li^{3+}-He collision are shown in Fig. 3. We see that the agreement with the experimental data [51,54-56] is excellent over the entire energy region. However, the results in postform of BCCIS-4B [32] (dashed curve) have good agreement with the findings of Shah and Gilbody [51] in the low-energy region (below 400 keV/amu). The reason may be due to the inclusion of continuum interaction of the active electron with the projectile ion of higher charge. The results of Belkic [57] (dash-dotted curve) obtained by CB1 method using an independent-particle model with the Rootham-Hartee-Fock target screening overestimate the present results in lower energy range (below 150 keV/amu). This may be due to the exclusion of many-body effects in this formalism. However, the results of Mancev [58] obtained by CDW-4B (dotted curve) underestimate the experimental results as well as present theoretical results in the whole energy range. In this calculation, they neglect the contributions of cross sections from hydrogenlike excited states and this underestimation may be attributed to this omission. The obtained theoretical findings for B^{5+}-He collision are plotted in Fig. 4. TCS results for the present FC-DW-4B and post BCCIS-4B are compared with other available measurements [59,60] and the theoretical data [10,60]. As can be seen in this figure, the BCCIS-4B results

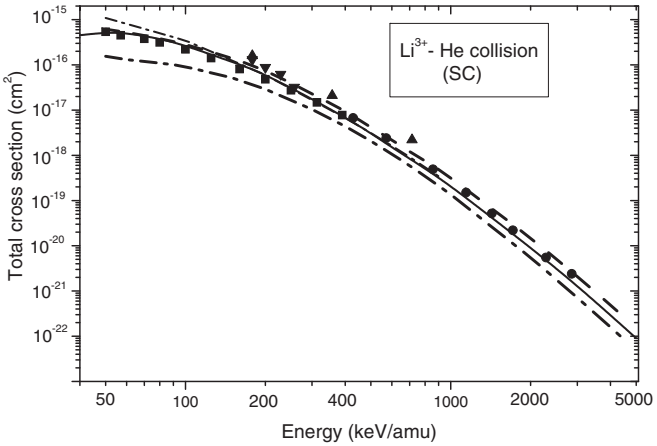

FIG. 3. Variation of total cross sections (TCS) for SC as a function of incident projectile energy for Li^{3+}-He collision. The solid curve presents FC-DW-4B results; dashed curve, BCCIS-4B results [32]; dash-dotted curve, CB1 results [57]; dash-dot-dotted curve, CDW-4B results [58]. Experimental data: solid square, results of Shah and Gilbody [51]; solid circle, results of Woitke *et al.* [54]; solid up triangle, results of Nikolaev *et al.* [55]; solid down triangle, results of Pivovar *et al.* [56].

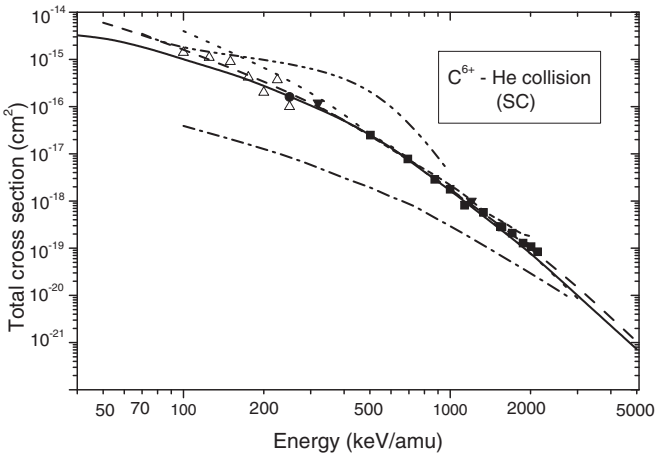

FIG. 5. Variation of total cross sections (TCS) for SC as a function of incident projectile energy for C^{6+}-He collision. The solid line presents FC-DW-4B results; dashed curve, BCCIS-4B results [32]; dash-dotted curve, BDW-3B results [10]; dotted curve, CDW-EFS-3B results [65], dash-dot-dotted curve, UDWA results [66]; short-dashed curve, atomic-orbital-expansion results [68]. Experimental data: solid circle, results of Guffey *et al.* [62]; solid square, results of Dillinghan [64]; solid down triangle, results of Graham *et al.* [63].

are much better than the present FC-DW-4B results in the lower-energy regime below 1 MeV/amu. With increase of energy the BCCIS-4B, the FC-DW-4B, and the three-body continuum distorted wave-eikonal final state (CDW-EFS-3B) [61] results have a converging trend. Here the CDW-EFS-3B results have excellent agreement with the experimental results of Dmitriev *et al.* [59] and Hippler *et al.* [60], whereas the prior form of BDW-3B [10] results underestimate both the experimental data. It may be noted that the prior form of both

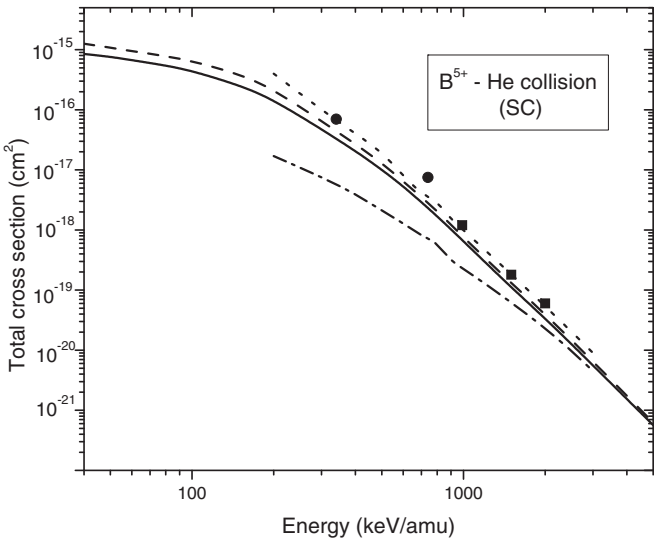

FIG. 4. Variation of total cross sections (TCS) for SC as a function of incident projectile energy for B^{5+}-He collision. The solid curve presents FC-DW-4B results; dashed curve, BCCIS-4B results [32]; dotted curve, CDW-EFS-3B results [61]; dashed curve, BDW-3B results [10]. Experimental data: solid circle, results of Dmitriev *et al.* [59]; solid square, results of Hippler *et al.* [60].

BDW-3B and CDW-EFS-3B models include the full Coulomb continuum intermediate states in the entrance channel. The numerical computations of the TCS for C^{6+}-He collision are carried out in the energy interval 40 keV/amu to 5 MeV/amu and the corresponding results are given in Fig. 5. A comparison between the present FC-DW-4B approximation and numerous experimental data [62-64] shown in this figure reveals overall good agreement. It is also observed that the present results of the FC-DW-4B method provide very similar cross sections as those by BCCIS-4B theory (dashed curve) at higher impact energies, but at lower energies the present FC-DW-4B results are smaller than the corresponding results of the BCCIS-4B [32] model. However, the TCS of the BDW-3B [10] (dash-dotted curve), CDW-EFS-3B [65] (dotted curve), unitarized-distorted-wave approximation [66] (dash-dot-dotted curve), and present theories (BCCIS-4B, FC-DW-4B) are closer to the experimental results [62-64] with increasing the projectile energy. The BDW-3B results underestimate the present results to a large extent at all energies. This may be due to the exclusion of the many-body effect which is very much important at low and intermediate energies. The agreement of the present cross sections with the results of the classical trajectory Monte Carlo (CTMC) method of Olson [67] and the atomic-orbital expansion of Jain *et al.* [68] are satisfactory in the whole energy range. However, the results of Suzuki *et al.* [66] obtained by the UDWA are much higher than the present results in the energy range of 400–700 keV/amu. For O^{8+}-He collisions, the present computed results are plotted in graphical form in Fig. 6. We have compared our theoretical results with a number of experimental results [60,62,64,69,70] and theoretical results [66-68]. From the figure, it is evident that the computed cross sections by means of the present FC-DW-4B approximation as well as the BCCIS-4B [32] have good agreement with the experimental results of Hippler *et al.* [60] and Macdonald and Martin [69] at high impact energies. The BCCIS-4B findings

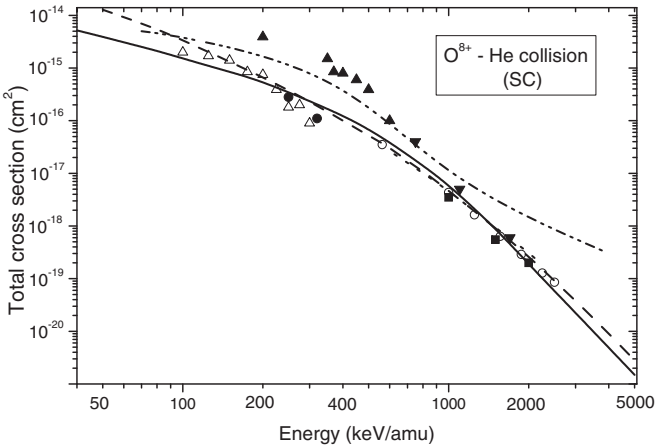

FIG. 6. Variation of total cross sections (TCS) for SC as a function of incident projectile energy for O^{8+}-He collision. The solid curve presents FC-DW-4B results; dashed curve, BCCIS-4B results [32]; dash-dot-dotted curve, UDWA results [66]; dotted curve, atomic-orbital-expansion results [68]; open up triangle, CTMC results [67]. Experimental data: solid circle, results of Guffey *et al.* [62]; solid square, results of Hippler [60]; solid up triangle, results of Afrosimov *et al.* [70]; solid down triangle, results of Macdonald and Martin [69]; open circle, results of Dillinghan *et al.* [64].

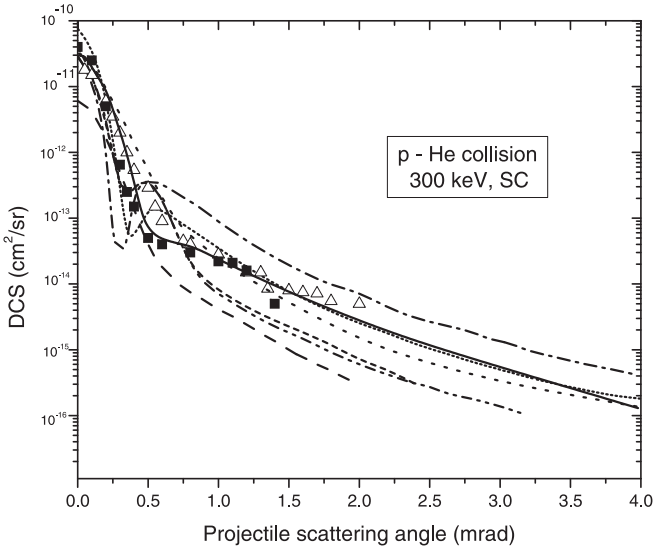

FIG. 7. Differential cross sections for SC in p-He collision as a function of projectile scattering angle for the incident energy of 300 keV. The solid curve presents FC-DW-4B results; dashed curve, BCCIS-4B results (postform) [32]; dash-dot-dotted curve, CDW-BFS results [42]; dotted curve, TCDW-4B results [49]; dash-dotted curve, CBDW-4B results [36]; short-dashed curve, BDW-4B results [21]; short-dotted curve, CBDW-3B results [38]. Experimental data: solid square, results of Mergel *et al.* [72]; open up triangle, results of Abufuger *et al.* [71].

overestimate the present results in the low impact energies where there was no experimental data for comparison.

B. Differential cross sections

1. Process involving SC

Next we turn our attention to differential cross sections (DCS) for the process involving SC which provides a more sensitive test for the theoretical models. At high impact energies, the DCS can always be divided into three angular regions where different mechanisms occur: (i) the small angles scattering region corresponding to forward scattering that extends up to the position of first dip at dark angle; (ii) the double scattering region centered on the Thomas angle where the electron is captured after undergoing two binary collisions; (iii) the large angles scattering region corresponding to close encounter collisions, where a rapid monotonic decrease is predicted. Of particular interest in high collision energies is the second angular region because the Thomas two-step process becomes dominant as the impact energy increases. The differential cross sections (DCS) for single electron capture by means of postform of the BCCIS-4B [32-34] and the present FC-DW-4B method are shown in Figs. 7–11 for p-He collision at energies 0.3, 1.3, 5, and 7.5 MeV, respectively. The shape of the distributions has three maxima at projectile scattering angle $\theta_p = 0$, secondary maxima at the expected Thomas angle, 0.47 mrad, and third maxima at 0.75 mrad, respectively, when the incident projectile energy is high. The results from the present FC-DW-4B method for DCS at 300 keV for p-He collision are shown in Fig. 7. Here the solid curve and dashed curve correspond to FC-DW-4B and BCCIS-4B (postform) results, respectively. The present results in both methods are compared with two sets of experimental measurements [71,72] and other theoretical data [21,36,38,42,49]. It may be seen from Fig. 7 that the present results have excellent agreement with the experimental results of Mergel *et al.* [72] in the whole range of projectile scattering angles. However, the DCS obtained by BCCIS-4B [34] are not in good agreement in the projectile scattering angle above the Thomas angle. We find the unphysical dip around the Thomas peak obtained by BDW-4B [21] (short-dashed curve), CBDW-4B [36] (dash-dotted curve), CBDW-3B [38] (short-dotted curve), and CDW-BFS [42] (dash-dot-dotted curve), respectively, which may be due to the mutual cancellation of potential terms. As can be seen from this figure, the DCS obtained by TCDW-4B [49] (dotted curve) are not in good agreement with experiments [71,72] in the wide range of projectile scattering angles with the exception from 1 mrad to 1.5 mrad. This model includes only the continuum state of the active electron with the target in the exit channel. Previously many theoretical models on ion-atom collisions concluded that the Thomas peak should appear exclusively at high projectile energies. But the present FC-DW-4B model predicts the Thomas peak at intermediate energy (300 keV) and high impact energies (shown later). At 300 keV, there is a hint of the double-scattering effect appearing as a left-sided shoulder of the Thomas peak. In Figs. 8–10, we present the results of proton-helium collisions in the form of the projectile differential cross sections at high impact energies (1.3, 5, and 7.5 MeV). We compare our theoretical data obtained by both FC-DW-4B and BCCIS-4B with those of the experimental results of Fischer *et al.* [73] and other theoretical results of Mancev *et al.* [30] obtained by the BCIS-4B method. It is seen that the shapes of the DCS as predicted by the present BCCIS-4B and FC-DW-4B along with BCIS-4B method of Mancev *et al.* [30] have a

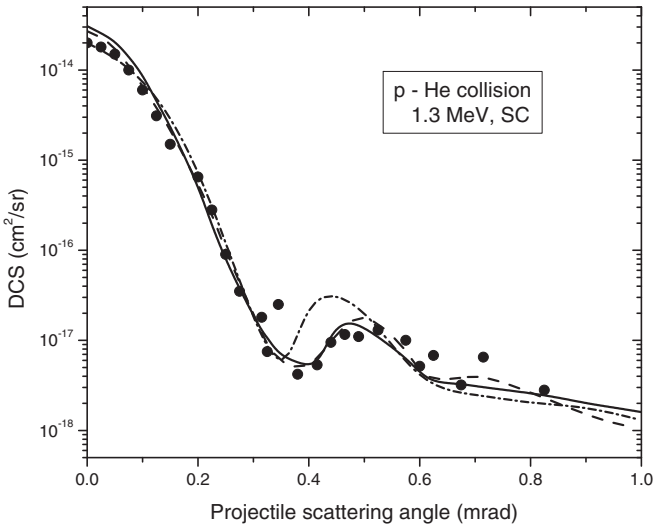

FIG. 8. Same as in Fig. 7. except for the incident energy of 1.3 MeV. The solid curve presents FC-DW-4B results; dashed curve, BCCIS-4B results (postform) [32]; short-dashed curve represents the results obtained by the prior form of the BCIS-4B method [30]. Experimental data: solid circle, results of Fischer *et al.* [73].

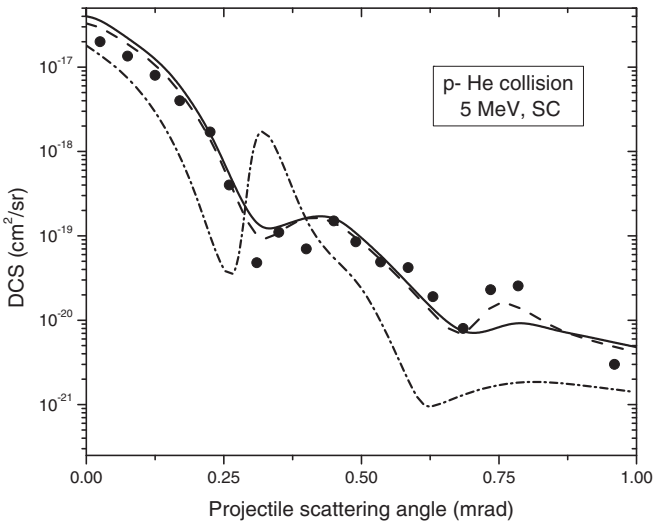

FIG. 9. Same as in Fig. 8. except for the incident energy of 5 MeV.

similar trend to the experimental data [73]. All these results have maxima at the forward angle ($\theta_p = 0$) as well as the Thomas peak located at about 0.47 mrad, which has been first observed experimentally by Horsdal-Pedersen *et al.* [74] for p-He collision at high projectile energies. The Thomas process may be accounted for by both classical [75] and quantum mechanical second Born descriptions [76]. In the classical picture [75], the projectile proton (p) scatters one of the active electrons in the target in such a way that this electron is being scattered by the target nucleus (N) and finally becomes bound to the projectile. This is called proton (p-e-N)Thomas double scattering and the Thomas angle is determined by $(\theta)_{p-e-N} = \frac{\sqrt{3}}{2}\frac{m_e}{M_P}$, which is independent of the projectile velocity and the target mass. It is also noted that in addition to the Thomas peak, another peak at $\theta_P \approx 0.75$ mrad, which is called broadband peak as mentioned by Mancev *et al.* [30], is observed in our present theoretical calculation at high impact energies as shown in Figs. 8–10. This feature has been verified experimentally by Fischer *et al.* [73]. However, the order of magnitude is less compared to the experimental data. We see that, with increasing projectile energies from 1.3 to 7.5 MeV, our theoretical results obtained by both BCCIS-4B and FC-DW-4B show clear peak at around 0.75 mrad, whereas the BCIS-4B [30] shows almost flat around the third peak (0.75 mrad). It is evident from Figs. 9 and 10 that, with increasing projectile energy, the BCCIS-4B results are slightly in better agreement with experiment [73] than those of FC-DW-4B results especially around the third peak at 0.75 mrad. The Thomas peak at 0.47 mrad for the double-scattering process p-e-N is much stronger than the third peak at 0.75 mrad. Finally, the Thomas and the third peak are separated by the second dip at about 0.687 mrad. However, beyond the double-scattering Thomas processes, other more complicated collision sequences modify the projectile's direction and may also lead to characteristic structures. The contributions of angular distribution from different terms of perturbation potential are shown in Fig. 11 for 7.5 MeV proton energy only. We find that one of the parts in V_f say the potential $V_2 = \frac{1}{r_{12}} - \frac{1}{s_2}$ in postform of BCCIS-4B [32] including correlation ($\frac{1}{r_{12}}$) along with the term of attractive potential ($-\frac{1}{s_2}$) between projectile and passive electron in the target (short dotted) gives less contribution compared to the other term say $V_1 = Z_T(\frac{1}{R} - \frac{1}{x_1})$ (short dashed) in the whole range of projectile scattering angles. This may be due to the fact that the potential $\frac{1}{r_{12}}$ in V_2 of BCCIS-4B (postform) represents the direct Coulomb interaction between e_1 and e_2 and the asymptotic tail is $\frac{1}{s_2}$, since $r_{12} \to s_2$ at infinitely large s_2 and finite s_1. As such, V_2 is a short-range interaction in accordance with the correct boundary conditions [16,27]. Therefore, we say that the dynamic correlation is comparatively less important. On the other hand, the angular distribution due to two components

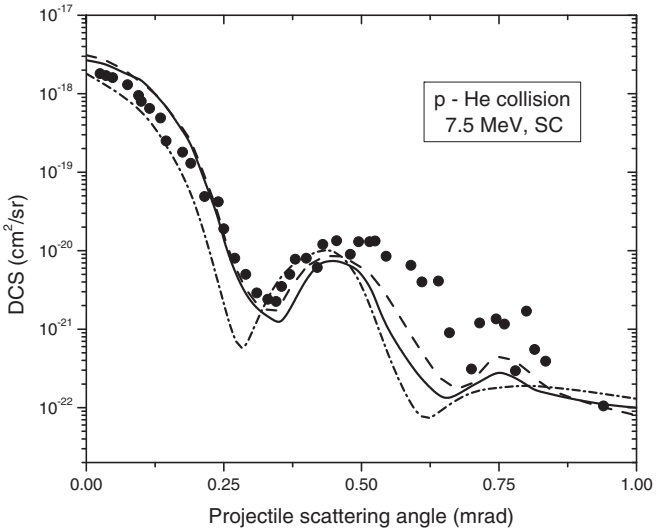

FIG. 10. Same as in Fig. 8. except for the incident energy of 7.5 MeV.

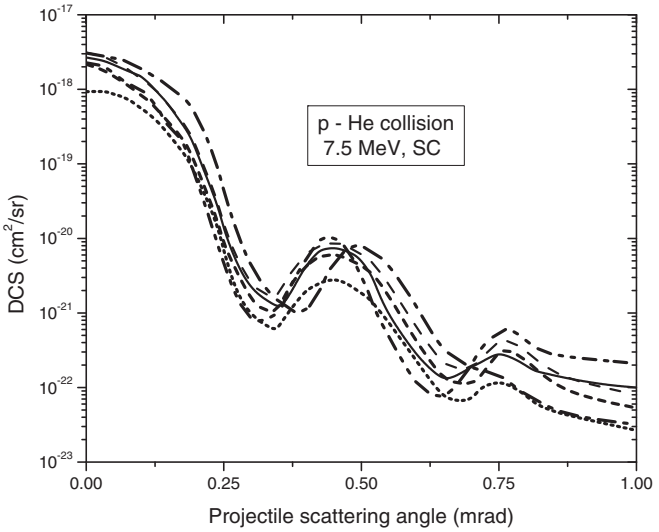

FIG. 11. DCS contributions from different terms of the potential in the total perturbation potential of the post BCCIS-4B and FC-DW-4B methods at incident projectile energy 7.5 MeV. In the post BCCIS-4B method, the short-dashed curve [$V_1 = Z_T(\frac{1}{R} - \frac{1}{x_1})$], short-dotted curve ($V_2 = \frac{1}{r_{12}} - \frac{1}{s_2}$), and dashed curve $V_t = V_1 + V_2$ and, in the FC-DW-4B method, the dash-dotted curve $V_1' = -\frac{Z_P}{s_1}$, dash-dot-dotted curve $V_2' = \frac{Z_P Z_T}{R}$, and solid curve $V_t' = V_1' + V_2'$.

$\frac{Z_P Z_T}{R}$, $-\frac{Z_P}{s_1}$ of the perturbation potential in the present FC-DW-4B model is also shown in this figure. The second term due to attractive potential ($-\frac{Z_T}{s_1}$) does not show the third peak, whereas the first component due to repulsive potential $\frac{Z_P Z_T}{R}$ describes the Rutherford scattering with peak structure which dominates at larger scattering angle in differential cross sections. The contribution of the third term $-\frac{Z_P}{s_2}$ gives very small contribution which is not shown here. These structures were also observed by Mancev *et al.* [30].

2. *Process involving TE*

SC has been studied extensively over many years, but few theoretical and experimental results on DCS for the two electron transfer-excitation (TE) process have been reported which was elaborately explained by Belkic [77]. So we can imagine that a variety of mechanisms such as *p-e-e* Thomas or shake processes may contribute to TE. In Figs. 12–14, we have shown our present results calculated by FC-DW-4B (solid curve), both BCCIS-4B (post) (dashed curve) and BCCIS-4B (prior) (dash-dot-dotted curve) together with previous different theoretical calculations by means of TC-BGM [25] (dotted curve) and nonperturbative time-dependent calculations (dash-dotted curve) based on the basic generator method [40] and the measurements [40,44] for p-He collision at projectile energies of 50, 75, and 100 keV, respectively. In these calculations, we have accounted for capture to the ground state of hydrogenlike atom and have summed over all final target states up to the $n = 2$ shell. It is observed that the present computed results using FC-DW-4B method are overall in good agreement with the experimental data [40,44] as compared to the other theoretical models in the wide range of scattering angles. As

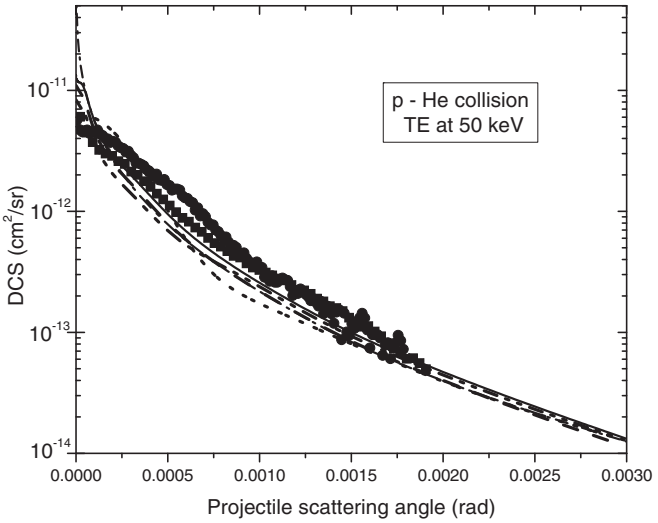

FIG. 12. Differential cross sections for TE in p-He collisions as a function of projectile scattering angle for the incident energy of 50 keV. The solid and dashed curves represent the FC-DW-4B and BCCIS-4B (post) results; dash-dot-dotted curve, BCCIS-4B (prior) results; dotted curve, TC-BGM results [25]; dash-dotted curve, results using nonperturbative calculation [40]. Experimental data: solid square, results of Guo *et al.* [73]; solid circle, results of Hasan *et al.* [40].

can be seen from Fig. 12, the FC-DW-4B results and the BCCIS-4B (post and prior) results largely overestimate the experimental data near zero degree emission angle. Also for 75 and 100 keV energies, the results obtained by BCCIS-4B in postform underestimate the experimental findings [40,44] in the whole range of projectile scattering angles. Despite the obvious discrepancy between V_i and V_f in BCCIS-4B [32], computations show that the post-prior discrepancy is within 25%. We see that the prior BCCIS-4B results is less than the postresults in the wide range of scattering angles except for the large projectile scattering angle. This may be

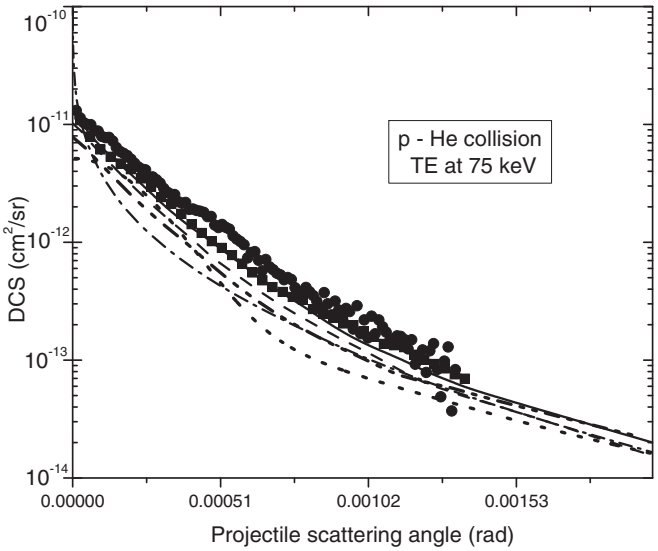

FIG. 13. Same as in Fig. 12, except for the incident energy of 75 keV.

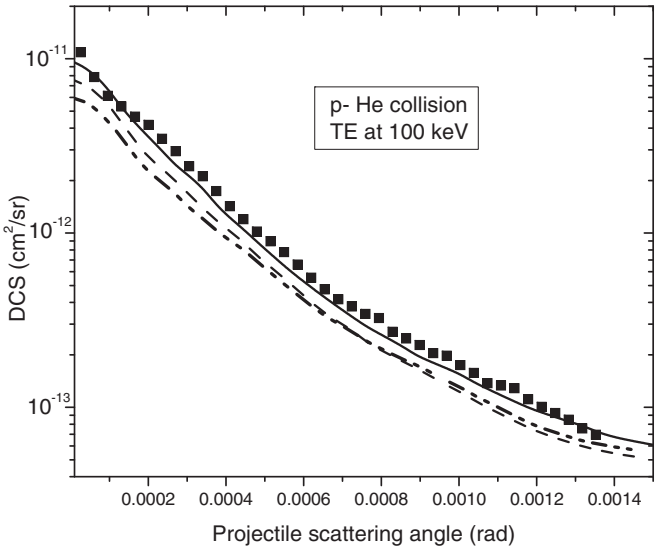

FIG. 14. Same as in Fig. 12. except for the incident energy of 100 keV.

due to the fact that the BCCIS-4B model both post and prior form does not include the Coulomb distortion between the projectile ion and the other noncaptured electron which may end up in the excited state of the target in the final channel, whereas the present FC-DW-4B model includes this distortion. The TC-BGM calculations based on the independent electron model (IEM) do not reproduce the experimental results. It is evident that the inclusion of Coulomb distortion between the projectile ion and the passive electron may play a significant role in TE processes and, as such, FC-DW-4B is so successful in reproducing experimental results.

IV. CONCLUSION

In the framework of the four-body model of distorted wave in final channel (FC-DW-4B) and boundary corrected continuum intermediate-state (BCCIS-4B) approximation, the total cross sections (TCS) and differential cross sections for SC and TE processes in collisions of bare ions with helium atoms in ground state have been extensively studied at intermediate and high energies. In the FC-DW-4B method, the dynamic electron correction is not included, whereas in the BCCIS-4B method, such correlation is automatically included through the perturbation potential. The TCS results so obtained are reasonably encouraging over the entire range of energy. It is also observed that the results obtained by the present model are encouraging over the postform of BCCIS-4B approximation at intermediate energy where projectile velocity is comparable to the orbital velocity. However, the electron-correlation effects are insignificant in this energy region. Numerical computations of the DCS for p-He collision are performed at one intermediate energy (300 keV) and three high projectile energies (1.3 MeV, 5 MeV, and 7.5 MeV), respectively. At projectile energy 300 keV, the FC-DW-4B results exhibit an interatomic double-scattering effect appearing as a shoulder of the Thomas peak around 0.5 mrad which is not found in post BCCIS-4B results. Further, the Thomas peak becomes clearly visible and thereafter, with increase of the impact energy, the Thomas peak becomes more pronounced in both the calculations (the present FC-DW-4B and BCCIS-4B). It is also noted that at high impact energies, the angular distribution of scattered projectile for the SC process revealed a third peak at 0.75 mrad in addition to the p-e-N peak (at around 0.47 mrad). This is called the broadband peak as mentioned by Mancev *et al.* [30]. This structure is clearly visible in the postresults of BCCIS-4B approximation and the present FC-DW-4B model, but the order of magnitude of FC-DW-4B is less than the BCCIS-4B (post). We have also investigated the transfer-excitation for p-He collision at different projectile energies (50, 75, and 100 keV). The obtained DCS by present FC-DW-4B are in excellent agreement with the recent experimental data. In this investigation, we may mention that the inclusion of distortion between the projectile and noncaptured electron in the target is very much important in the TE process because the residual electron in the target may be excited. Inclusion of this feature is absent in the BCCIS-4B approximation. Overall, the present thorough analysis shows that the BCCIS-4B and FC-DW-4B models can confidently be explored for many collision dynamics of SC and TE process in ion-atom collisions and can also be further extended to the FC-DW-4B model.

ACKNOWLEDGMENTS

The authors gratefully acknowledge the financial support from the Council of Scientific & Industrial Research (CSIR), New Delhi, India through Project No. 03/1366/16/EMR-II. We thank Professor M. Schulz and Professor X. Ma for providing us with experimental data.

[1] J. R. Oppenheimer, Phys. Rev. **31**, 349 (1928).
[2] J. D. Jackson and H. Schiff, Phys. Rev. **89**, 359 (1953).
[3] D. P. Dewangan and J. K. M. Eichler, J. Phys. B: At., Mol., Opt. Phys. **19**, 2939 (1986).
[4] S. Saini and D. Farrelly, Phys. Rev. A **36**, 3556 (1987).
[5] G. C. Saha, S. Datta, and S. C. Mukherjee, Phys. Rev. A **36**, 1656 (1987).
[6] M. Purkait, Nucl. Instrum. Methods, Phys. Res. B **207**, 101 (2003).
[7] M. Das, M. Purkait, and C. R. Mandal, Phys. Rev. A **57**, 3573 (1998).
[8] M. Purkait, M. Das, and C. R. Mandal, Phys. Rev. A **60**, 3025 (1999).
[9] M. E. Galassi, P. N. Abufager, A. E. Martinez, R. D. Rivarola, and P. D. Fainstin, J. Phys. B: At., Mol., Opt. Phys. **35**, 1727 (2002).
[10] M. Rahmanian, F. Shojaei, and R. Fathi, J. Phys. B: At., Mol., Opt. Phys. **49**, 175201 (2016).
[11] R. Samanta and M. Purkait, Phys. Scr. **82**, 065303 (2010).
[12] G. C. Saha, S. Datta, and S. C. Mukherjee, Phys. Rev. A **34**, 2809 (1986).
[13] Dz. Belkic, R. Gayet, and A. Salin, Phys. Rep. **56**, 279 (1979).

[14] B. H. Bransden and M. R. C. McDowell, *Charge Exchange and the Theory of Ion-Atom Collisions*, International Series of Monographs in Physics (Clarendon, Oxford, 1992).
[15] D. P. Dewangan and J. Eichler, Phys. Rep. **247**, 59 (1994).
[16] Dz. Belkic, *Principles of Quantum Scattering Theory* (Institute of Physics, Bristol, UK, 2003).
[17] Dz. Belkic, *Quantum Theory of High-Energy Ion-Atom Collisions* (Taylor and Francis, London, 2008).
[18] Dz. Belkic, R. Gayet, J. Hanssen, I. Mancev, and A. Nunez, Phys. Rev. A **56**, 3675 (1997).
[19] I. Mancev, Phys. Rev. A **75**, 052716 (2007).
[20] I. Mancev, J. Phys. B: At., Mol., Opt. Phys. **36**, 93 (2003).
[21] I. Mancev, V. Mergel, and L. Schmidt, J. Phys. B: At., Mol., Opt. Phys. **36**, 2733 (2003).
[22] P. N. Abufager, A. E. Martinez, R. D. Rivarola, and P. D. Fainsteins, J. Phys. B: At., Mol., Opt. Phys. **37**, 817 (2004).
[23] I. Mancev, Europhys. Lett. **69**, 200 (2005).
[24] I. Mancev, J. Comput. Methods Sci. Eng. **5**, 73 (2005).
[25] M. Zapukhlyak, T. Kirchner, A. Hasan, B. Tooke, and M. Schulz, Phys. Rev. A **77**, 012720 (2008).
[26] M. Zapukhlyak and T. Kirchner, Phys. Rev. A **80**, 062705 (2009).
[27] I. Mancev and N. Milojevic, Phys. Rev. A **81**, 022710 (2010).
[28] I. Mancev, N. Milojevic, and Dz. Belkic, Phys. Rev. A **86**, 022704 (2012).
[29] I. Mancev, N. Milojevic, and Dz. Belkic, Phys. Rev. A **88**, 052706 (2013).
[30] I. Mancev, N. Milojevic, and Dz. Belkic, Phys. Rev. A **91**, 062705 (2015).
[31] R. Samanta and M. Purkait, Eur. Phys. J. D **64**, 311 (2011).
[32] R. Samanta, M. Purkait, and C. R. Mandal, Phys. Rev. A **83**, 032706 (2011).
[33] R. Samanta, S. Jana, C. R. Mandal, and M. Purkait, Phys. Rev. A **85**, 032714 (2012).
[34] R. Samanta and M. Purkait, Phys. Scr. **84**, 065301 (2011).
[35] S. Jana and M. Purkait, Indian J Phys. **88**, 343 (2014).
[36] E. Ghanbari-Adivi and H. Ghavaminia, Phys. Scr. **89**, 105402 (2014).
[37] E. Ghanbari-Adivi and H. Ghavaminia, J. Phys. B: At., Mol., Opt. Phys. **45**, 235202 (2012).
[38] E. Ghanbari-Adivi, J. Phys. B: At., Mol., Opt. Phys. **44**, 165204 (2011).
[39] D. Fischer, K. Støchkel, H. Cederquist, H. Zettergren, P. Reinhed, R. Schuch, A. Källberg, A. Simonsson, and H. T. Schmidt, Phys. Rev. A **73**, 052713 (2006).
[40] A. Hasan, B. Tooke, M. Zapukhlyak, T. Kirchner, and M. Schulz, Phys. Rev. A **74**, 032703 (2006).
[41] M. Schulz, T. Vajnai, and J. A. Brand, Phys. Rev. A **75**, 022717 (2007).
[42] M. S. Schoffler, J. Titze, L. Ph. H. Schmidt, T. Jahnke, N. Neumann, O. Jagutzki, H. Schmidt-Bocking, R. Dorner, and I. Mancev, Phys. Rev. A **79**, 064701 (2009).
[43] M. S. Schöffler, J. N. Titze, L. Ph. H. Schmidt, T. Jahnke, O. Jagutzki, H. Schmidt-Böcking, and R. Dörner, Phys. Rev. A **80**, 042702 (2009).
[44] D. L. Guo, X. Ma, S. F. Zhang, X. L. Zhu, W. T. Feng, R. T. Zhang, B. Li, H. P. Liu, S. C. Yan, P. J. Zhang, and Q. Wang, Phys. Rev. A **86**, 052707 (2012).
[45] P. Lowdin, Phys. Rev. **90**, 120 (1953).
[46] A. Nordsieck, Phys. Rev. **93**, 785 (1954).
[47] R. R. Lewis, Phys. Rev. **102**, 537 (1956).
[48] C. Sinha and N. C. Sil, J. Phys. B **11**, 1807 (1978).
[49] S. Samaddar, S. Halder, A. Mondal, C. R. Mondal, M. Purkait, and T. K Das, J. Phys. B: At., Mol., Opt. Phys. **50**, 065202 (2017).
[50] M. B. Shah, P. McCallion, and H. B. Gilbody, J. Phys. B: At., Mol., Opt. Phys. **22**, 3037 (1989).
[51] M. B. Shah and H. B. Gilbody, J. Phys. B: At., Mol., Opt. Phys. **18**, 899 (1985).
[52] N. V. de Castro Faria, F. L. Freire, Jr., and A. G. de Pinho, Phys. Rev. A **37**, 280 (1988).
[53] I. Mančev, Phys. Rev. A **60**, 351 (1999).
[54] O. Woitke, P. A. Zavodszky, S. M. Ferguson, J. H. Houck, and J. A. Tanis, Phys. Rev. A **57**, 2692 (1998).
[55] V. S. Nikolaev, I. S. Dmitriev, L. N. Fateeva, and Yu. A. Teplova, Sov. Phys. JETP **13**, 695 (1961) [Zh. Eksp. Teor. Fiz. **40**, 989 (1961)].
[56] L. I. Pivovar, Yu. Z. Levchenko, and G. A. Krivonosov, Sov. Phys. JETP **32**, 11 (1971) [Zh. Eksp. Teor. Fiz. **59**, 19 (1970)].
[57] Dz. Belkic, Phys. Scr. **40**, 610 (1989).
[58] I. Mancev, Phys. Rev. A **64**, 012708 (2001).
[59] I. S. Dmitriev, Ya. A. Teplova, Ya. A. Belkova, N. V. Novikov, and Yu. A. Fainberg, At. Data Nucl. Data Tables **96**, 85 (2010).
[60] R. Hippler, S. Datz, P. D. Miller, P. L. Pepmiller, and P. F. Dittner, Phys. Rev. A **35**, 585 (1987).
[61] H. F. Busnengo, S. E. Cochs, A. E. Martinez, and R. D. Rivarola, Phys. Scr. **T62**, 88 (1996).
[62] J. A. Guffey, L. D. Ellsworth, and J. R. Macdonald, Phys. Rev. A **15**, 1863 (1977).
[63] W. G. Graham, K. H. Berkner, R. V. Pyle, A. S. Schlachter, J. W. Stearns, and J. A. Tanis, Phys. Rev. A **30**, 722 (1984).
[64] T. R. Dillingham, J. R. Macdonald, and P. Richard, Phys. Rev. A **24**, 1237 (1981).
[65] H. F. Busnengo, S. E. Corchs, A. E. Martinez, and R. D. Rivarola, Phys. Scr. **T73**, 242 (1997).
[66] H. Suzuki, Y. Kajikawa, N. Toshima, H. Ryufuku, and T. Watanabe, Phys. Rev. A **29**, 525 (1984).
[67] R. E. Olson, Phys. Rev. A **18**, 2464 (1978).
[68] A. Jain, C. D. Lin, and W. Fritsch, Phys. Rev. A **34**, 3676 (1986).
[69] R. Macdonald and F. W. Martin, Phys. Rev. A **4**, 1965 (1971).
[70] V. V. Afrosimov, A. A. Basalaev, E. D. Donets, K. O. Lozhkin, and M. N. Panov, in *Abstracts of the Twelfth International Conferences on the Physics of Electronic and Atomic Collisions, Gatlinburg, Tennessee*, edited by S. Datz (North-Holland, Amsterdam, 1981), p. 690.
[71] P. N. Abufuger, P. D. Fainstein, A. E. Martinez, and R. D. Rivarola, J. Phys. B: At., Mol., Opt. Phys. **38**, 11 (2005).
[72] V. Mergel, R. Dörner, K. Khayyat, M. Achler, T. Weber, O. Jagutzki, H. J. Lüdde, C. L. Cocke, and H. Schmidt-Böcking, Phys. Rev. Lett. **86**, 2257 (2001).
[73] D. Fischer, M. Gudmundsson, Z. Berenyi, N. Haag, H. A. B. Johansson, D. Misra, P. Reinhed, A. Kallberg, A. Simonsson, K. Stochkel, H. Cederquist, and H. T. Schmidt, Phys. Rev. A **81**, 012714 (2010).
[74] E. Horsdal-Pedersen, C. L. Cocke, and M. Stockli, Phys. Rev. Lett. **50**, 1910 (1983).
[75] L. H. Thomas, Proc. R. Soc. **114**, 561 (1927).
[76] R. M. Drisko, Ph.D. thesis, Carnegie Institute of Technology, 1955.
[77] Dz. Belkic, I. Mancev, and J. Hanssen, Rev. Mod. Phys. **80**, 249 (2008).